Featured in Physics

Broadband Quantum Enhancement of the LIGO Detectors with Frequency-Dependent Squeezing

D. Ganapathy,[1,*] W. Jia,[1,*] M. Nakano,[2,*] V. Xu,[1,*] N. Aritomi,[3] T. Cullen,[4] N. Kijbunchoo,[5] S. E. Dwyer,[3] A. Mullavey,[2] L. McCuller,[4] R. Abbott,[4] I. Abouelfettouh,[3] R. X. Adhikari,[4] A. Ananyeva,[4] S. Appert,[4] K. Arai,[4] S. M. Aston,[2] M. Ball,[6] S. W. Ballmer,[7] D. Barker,[3] L. Barsotti,[1,†] B. K. Berger,[9] J. Betzwieser,[2] D. Bhattacharjee,[8] G. Billingsley,[4] S. Biscans,[4,1] N. Bode,[10,11] E. Bonilla,[9] V. Bossilkov,[2] A. Branch,[2] A. F. Brooks,[4] D. D. Brown,[12] J. Bryant,[13] C. Cahillane,[7] H. Cao,[14] E. Capote,[7] F. Clara,[3] J. Collins,[2] C. M. Compton,[3] R. Cottingham,[2] D. C. Coyne,[4] R. Crouch,[3] J. Csizmazia,[3] L. P. Dartez,[3] N. Demos,[1] E. Dohmen,[3] J. C. Driggers,[3] A. Effler,[2] A. Ejlli,[15] T. Etzel,[4] M. Evans,[1] J. Feicht,[4] R. Frey,[6] W. Frischhertz,[2] P. Fritschel,[1] V. V. Frolov,[2] P. Fulda,[16] M. Fyffe,[2] B. Gateley,[3] J. A. Giaime,[17,2] K. D. Giardina,[2] J. Glanzer,[17] E. Goetz,[18] R. Goetz,[16] A. W. Goodwin-Jones,[19] S. Gras,[1] C. Gray,[3] D. Griffith,[4] H. Grote,[15] T. Guidry,[3] E. D. Hall,[1] J. Hanks,[3] J. Hanson,[2] M. C. Heintze,[2] A. F. Helmling-Cornell,[6] N. A. Holland,[20] D. Hoyland,[13] H. Y. Huang,[21] Y. Inoue,[21] A. L. James,[15] A. Jennings,[3] S. Karat,[4] S. Karki,[22] M. Kasprzack,[4] K. Kawabe,[3] P. J. King,[3] J. S. Kissel,[3] K. Komori,[1] A. Kontos,[23] R. Kumar,[3] K. Kuns,[1] M. Landry,[3] B. Lantz,[9] M. Laxen,[2] K. Lee,[24] M. Lesovsky,[4] F. Llamas,[25] M. Lormand,[2] H. A. Loughlin,[1] R. Macas,[26] M. MacInnis,[1] C. N. Makarem,[4] B. Mannix,[6] G. L. Mansell,[7,1] R. M. Martin,[27] K. Mason,[1] F. Matichard,[4] N. Mavalvala,[1] N. Maxwell,[3] G. McCarrol,[2] R. McCarthy,[3] D. E. McClelland,[28] S. McCormick,[2] T. McRae,[28] F. Mera,[3] E. L. Merilh,[2] F. Meylahn,[10,11] R. Mittleman,[1] D. Moraru,[3] G. Moreno,[3] T. J. N. Nelson,[2] A. Neunzert,[3] J. Notte,[27] J. Oberling,[3] T. O'Hanlon,[2] C. Osthelder,[4] D. J. Ottaway,[12] H. Overmier,[2] W. Parker,[2] A. Pele,[4] H. Pham,[2] M. Pirello,[3] V. Quetschke,[25] K. E. Ramirez,[2] J. Reyes,[27] J. W. Richardson,[14] M. Robinson,[3] J. G. Rollins,[4] C. L. Romel,[3] J. H. Romie,[2] M. P. Ross,[29] K. Ryan,[3] T. Sadecki,[3] A. Sanchez,[3] E. J. Sanchez,[4] L. E. Sanchez,[4] R. L. Savage,[3] D. Schaetzl,[4] M. G. Schiworski,[12] R. Schnabel,[30] R. M. S. Schofield,[6] E. Schwartz,[15] D. Sellers,[2] T. Shaffer,[3] R. W. Short,[3] D. Sigg,[3] B. J. J. Slagmolen,[28] C. Soike,[3] S. Soni,[1] V. Srivastava,[7] L. Sun,[28] D. B. Tanner,[16] M. Thomas,[2] P. Thomas,[3] K. A. Thorne,[2] C. I. Torrie,[4] G. Traylor,[2] A. S. Ubhi,[13] G. Vajente,[4] J. Vanosky,[4] A. Vecchio,[13] P. J. Veitch,[12] A. M. Vibhute,[3] E. R. G. von Reis,[3] J. Warner,[3] B. Weaver,[3] R. Weiss,[1] C. Whittle,[1] B. Willke,[10,11] C. C. Wipf,[4] H. Yamamoto,[4] L. Zhang,[4] and M. E. Zucker[1,4]

(LIGO O4 Detector Collaboration)

[1]*LIGO Laboratory, Massachusetts Institute of Technology, Cambridge, Massachusetts 02139, USA*
[2]*LIGO Livingston Observatory, Livingston, Louisiana 70754, USA*
[3]*LIGO Hanford Observatory, Richland, Washington 99352, USA*
[4]*LIGO Laboratory, California Institute of Technology, Pasadena, California 91125, USA*
[5]*OzGrav, School of Physical Sciences, University of Adelaide, Adelaide 5005, Australia*
[6]*University of Oregon, Eugene, Oregon 97403, USA*
[7]*Syracuse University, Syracuse, New York 13244, USA*
[8]*Kenyon College, Gambier, Ohio 43022, USA*
[9]*Stanford University, Stanford, California 94305, USA*
[10]*Max Planck Institute for Gravitational Physics (Albert Einstein Institute), D-30167 Hannover, Germany*
[11]*Leibniz Universität Hannover, D-30167 Hannover, Germany*
[12]*OzGrav, University of Adelaide, Adelaide, South Australia 5005, Australia*
[13]*University of Birmingham, Birmingham B15 2TT, United Kingdom*
[14]*University of California, Riverside, Riverside, California 92521, USA*
[15]*Cardiff University, Cardiff CF24 3AA, United Kingdom*
[16]*University of Florida, Gainesville, Florida 32611, USA*
[17]*Louisiana State University, Baton Rouge, Louisiana 70803, USA*
[18]*University of British Columbia, Vancouver, British Columbia V6T 1Z4, Canada*
[19]*OzGrav, University of Western Australia, Crawley, Western Australia 6009, Australia*
[20]*Vrije Universiteit Amsterdam, 1081 HV, Amsterdam, Netherlands*
[21]*National Central University, Taoyuan City 320317, Taiwan*
[22]*Missouri University of Science and Technology, Rolla, Missouri 65409, USA*
[23]*Bard College, Annandale-On-Hudson, New York 12504, USA*
[24]*Sungkyunkwan University, Seoul 03063, Republic of Korea*
[25]*The University of Texas Rio Grande Valley, Brownsville, Texas 78520, USA*
[26]*University of Portsmouth, Portsmouth, PO1 3FX, United Kingdom*
[27]*Montclair State University, Montclair, New Jersey 07043, USA*
[28]*OzGrav, Australian National University, Canberra, Australian Capital Territory 0200, Australia*

[29]*University of Washington, Seattle, Washington 98195, USA*
[30]*Universität Hamburg, D-22761 Hamburg, Germany*

(Received 15 April 2023; revised 22 July 2023; accepted 6 September 2023; published 30 October 2023)

Quantum noise imposes a fundamental limitation on the sensitivity of interferometric gravitational-wave detectors like LIGO, manifesting as shot noise and quantum radiation pressure noise. Here, we present the first realization of frequency-dependent squeezing in full-scale gravitational-wave detectors, resulting in the reduction of both shot noise and quantum radiation pressure noise, with broadband detector enhancement from tens of hertz to several kilohertz. In the LIGO Hanford detector, squeezing reduced the detector noise amplitude by a factor of 1.6 (4.0 dB) near 1 kHz; in the Livingston detector, the noise reduction was a factor of 1.9 (5.8 dB). These improvements directly impact LIGO's scientific output for high-frequency sources (e.g., binary neutron star postmerger physics). The improved low-frequency sensitivity, which boosted the detector range by 15%–18% with respect to no squeezing, corresponds to an increase in the astrophysical detection rate of up to 65%. Frequency-dependent squeezing was enabled by the addition of a 300-meter-long filter cavity to each detector as part of the LIGO A+ upgrade.

DOI: 10.1103/PhysRevX.13.041021 Subject Areas: Gravitation, Optics, Quantum Physics

I. INTRODUCTION

Interferometric gravitational-wave detectors are designed to be limited by quantum noise in most of their detection band from 20 Hz to a few kilohertz [1,2]. This measurement noise can be attributed to quantum fluctuations of the electromagnetic field that enters the interferometer at its readout port. These quantum fluctuations interact with the interferometer and return to the readout port, where they create noise on the readout photodetectors [3].

The quantum description of this interaction traditionally relies on two canonically conjugate operators: the phase and amplitude quadrature operators. In this description, the ground state of the electromagnetic field is a coherent state with zero average amplitude and equal uncertainty in both phase and amplitude. This state is known as the "coherent vacuum state," and the uncertainty in phase and amplitude are often referred to as quantum fluctuations or "vacuum fluctuations." Quantum noise in an interferometer can, thus, be described by two conceptually distinct components: shot noise, caused by phase quadrature vacuum fluctuations, and radiation pressure noise, caused by amplitude quadrature vacuum fluctuations.

Unlike the coherent vacuum state, squeezed vacuum states have reduced uncertainty in one quadrature and increased uncertainty in the other, as required by the Heisenberg uncertainty principle. Instead of allowing the coherent vacuum state to enter the interferometer, squeezed vacuum states (or simply "squeezing") can be injected into the readout port to reduce quantum noise and enhance the interferometer sensitivity to gravitational waves [4].

The GEO600 interferometer has employed squeezing since 2009 [5,6], and squeezing was also injected in the initial LIGO Hanford detector in 2011 [7]. In their third observing run (O3), the LIGO, Virgo, and GEO600 interferometers all employed squeezing to reduce shot noise [8–10]. These were implementations of "frequency-independent squeezing," where the injected squeezed vacuum states had reduced uncertainty in the phase quadrature, thus reducing shot noise at the expense of increased uncertainty in the amplitude quadrature and, consequently, increased radiation pressure noise [11,12]. With increasing laser power and higher levels of squeezing in the phase quadrature, radiation pressure noise can become dominant, preventing further sensitivity improvement beyond the point where the two forms of quantum noise are balanced. This limit is the primary motivation for the development of "frequency-dependent squeezing" and its implementation in LIGO, which is the focus of the work described here.

The history of gravitational-wave detectors is deeply linked with the study of how quantum processes impact precision measurement [13,14]. The term "nondemolition" was introduced to name techniques that circumvent or surpass the balancing act between competing quantum noise terms [15]. In the 1980s, state preparation was established as a nondemolition technique [16,17] that can achieve a broadband reduction of quantum noise [18]. To do so, a squeezed vacuum state must be prepared for phase squeezing in the shot-noise-limited region and

*These authors contributed equally to this work.
†lisabar@ligo.mit.edu

Published by the American Physical Society under the terms of the Creative Commons Attribution 4.0 International license. Further distribution of this work must maintain attribution to the author(s) and the published article's title, journal citation, and DOI.

amplitude squeezing in the region dominated by radiation pressure noise. Furthermore, quantum radiation pressure noise can be viewed as a consequence of backaction, resulting from the measurement of the interferometer's output field [19].

In 2001, Kimble *et al.* [20] proposed using a low-loss optical filter cavity, detuned from resonance, to impart the necessary frequency-dependent rotation of the squeezed states' quadrature before injection into the interferometer. Frequency-dependent squeezing circumvents backaction to enable a reduction of quantum noise over the entire astrophysical detection band. Several experimental groups have developed this technique [21–25] with the goal of meeting the strict requirements of gravitational-wave detectors [26–30]. Alternative techniques to reduce backaction through squeezing have also been experimentally demonstrated [31–33].

To implement frequency-dependent squeezing in LIGO, a 300-m-long filter cavity was installed at both the Hanford, Washington (H1) and Livingston, Louisiana (L1) interferometers as part of an upgrade program known as A+. Several other improvements to the squeezed state production and injection systems were also part of this upgrade, including low-loss optical components and active mode-matching elements [34–36]. These upgrades were implemented together to boost detector sensitivity for the fourth observing run (O4). Here, we report the first realization of frequency-dependent squeezing in gravitational-wave detectors, resulting in a broadband reduction of quantum noise and significant sensitivity improvement in both LIGO detectors.

II. THEORY

This section describes how the injection of frequency-dependent squeezing enables a broadband reduction of quantum noise in the LIGO interferometers [20,37]. For clarity, the simplified model of quantum noise presented here considers a lossless interferometer, operated on resonance.

The spectral behavior of quantum noise is usually described by a power spectral density calibrated in units of interferometer strain: S_h^{QN}. Without injected squeezing, S_h^{QN} is the sum of shot noise and quantum radiation pressure noise:

$$S_h^{\mathrm{QN}} = S_h^{\mathrm{SN}} + S_h^{\mathrm{RPN}}. \tag{1}$$

Shot noise S_h^{SN} decreases inversely with optical power and is given by

$$S_h^{\mathrm{SN}}(\Omega) = \frac{\hbar\gamma}{4kLP}\left(1+\frac{\Omega^2}{\gamma^2}\right), \tag{2}$$

where Ω is the angular measurement frequency, k is the wave number of 1064 nm interferometer light, $L = 4$ km is the arm cavity length, and $P \sim 350$ kW is the circulating laser power. LIGO interferometers use resonant cavities to enhance the arm power and strain sensitivity, which set the signal bandwidth to $\gamma \sim 2\pi \times 450$ Hz. By contrast, quantum radiation pressure increases linearly with the optical power, producing a strain noise power spectral density of

$$S_h^{\mathrm{RPN}}(\Omega) = \frac{64\hbar k P}{m^2 L^3 \gamma}\frac{1}{\Omega^4}\left(1+\frac{\Omega^2}{\gamma^2}\right)^{-1}, \tag{3}$$

where $m = 40$ kg is the mass of the suspended mirrors.

For the set of parameters above, the crossover where $S_h^{\mathrm{SN}}(\Omega) = S_h^{\mathrm{RPN}}(\Omega)$ is $\Omega = 2\pi \times 43$ Hz. This frequency increases with the circulating laser power and decreases with higher mirror mass.

Squeezing either phase or amplitude will suppress one of these noises by a factor of e^{2r} while amplifying the other by the same amount, where r is known as the squeeze factor. A squeezed state can be represented by an uncertainty ellipse in a space defined by two quadratures (Fig. 1, yellow panels), where the ellipse angle, or "squeeze angle," is determined by the relative phase between the squeezed field and the interferometer field. A change of this angle, thus the quadrature that is squeezed, can be described as a "rotation."

The optical and mechanical responses of the interferometer further shape the squeezed state interacting with it. The result is that the quantum noise of the interferometer with injected squeezing is described by [11,37]

$$S_h^{\mathrm{SQZ}} = S_h^{\mathrm{QN}}\left[e^{-2r}\cos^2[\phi-\theta(\Omega)] + e^{2r}\sin^2[\phi-\theta(\Omega)]\right], \tag{4}$$

where S_h^{QN} is the quantum noise without squeezing [Eq. (1)], ϕ is the squeezing angle relative to the readout quadrature, and $\theta(\Omega)$ arises from the optomechanical response of the interferometer:

$$\theta(\Omega) = \tan^{-1}\left[\frac{16kP}{mL\gamma}\frac{1}{\Omega^2}\left(1+\frac{\Omega^2}{\gamma^2}\right)^{-1}\right]. \tag{5}$$

When frequency-independent phase squeezing is injected, the above two equations simplify to

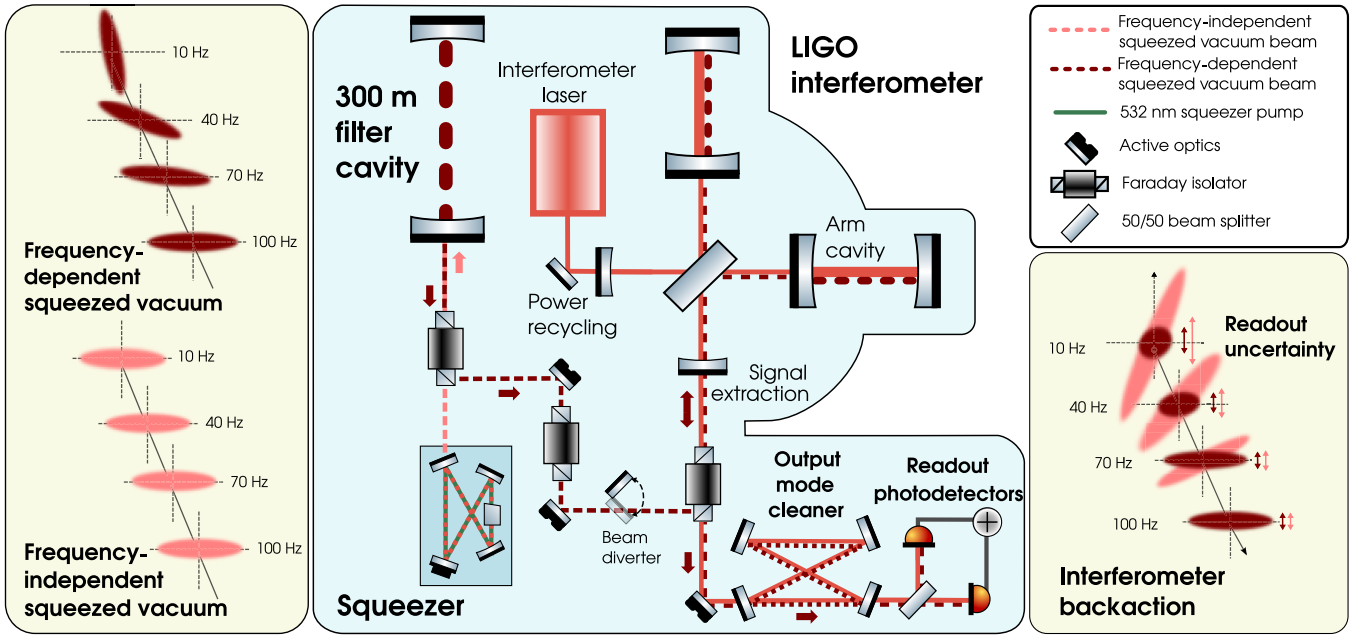

FIG. 1. Experimental setup of frequency-dependent squeezing in the LIGO detectors. The blue panel shows a simplified overview of the main experimental components. The LIGO detector is a modified Michelson interferometer with Fabry-Perot arm cavities and both power recycling and signal extraction cavities [1]. The LIGO squeezer [8] generates squeezed vacuum at 1064 nm using a subthreshold optical parametric oscillator, pumped at 532 nm. The squeezed beam reflects from the 300-m filter cavity, and a movable beam diverter opens to inject squeezing at the output port of the interferometer. Three Faraday isolators prevent stray interferometer light from reaching the squeezer and filter cavity. Active steering optics [34] enable alignment and mode matching of the squeezed beam to the filter cavity and interferometer. The squeezed beam copropagates with the outgoing interferometer beam through the output mode cleaner cavity, for measurement at the readout photodetectors [1]. The yellow panels illustrate uncertainty ellipses of squeezed states in phase space [20], where vacuum fluctuations are squeezed along the vertical readout quadrature. The left depicts the frequency-dependent rotation impressed by filter cavity resonance (upper) upon the generated squeezed vacuum state (lower). The right shows how the interferometer backaction affects the injected squeezed state, which is either frequency independent (light) or frequency dependent (dark). In either case, the ellipse is rotated and stretched, corresponding to rotation and gain of the squeezed state. For frequency-independent squeezing, uncertainty in the readout quadrature is increased at low frequencies, as indicated by the vertical red arrows. For frequency-dependent squeezing prepared with the appropriate rotation to counteract backaction, a reduced uncertainty in the readout quadrature is recovered at low frequencies.

$$S_h^{\mathrm{SQZ}}(\phi = 0) = e^{-2r} S_h^{\mathrm{SN}} + e^{2r} S_h^{\mathrm{RPN}}, \tag{6}$$

analogous to increasing the laser power by a factor of e^{2r}. In this case, $S_h^{\mathrm{SQZ}} > S_h^{\mathrm{QN}}$ for frequencies below approximately 100 Hz due to interferometer backaction from the e^{2r} enhanced radiation pressure term. When the injected squeezed states are instead prepared with frequency-dependent squeezing angles, $\phi(\Omega) = \theta(\Omega)$, the total quantum noise S_h^{SQZ} can be minimized to $e^{-2r} S_h^{\mathrm{QN}}$ across the detection band, analogous to increasing both laser power P and mirror mass m by a factor of e^{2r}. This is the premise of frequency-dependent squeezing—to overcome not one but two engineering challenges using quantum enhancement.

The appropriate frequency-dependent squeezing angles can be produced by reflecting the squeezed states off an optical filter cavity, detuned from the interferometer laser carrier frequency at $\Omega = 0$, before injection in the interferometer [20].

III. EXPERIMENTAL SETUP

Figure 1 shows the experimental implementation of frequency-dependent squeezing via a filter cavity in LIGO, with an overview of the full interferometer and key elements of the squeezing system. A more complete description of the squeezer experimental setup and control scheme is presented in Appendix A.

A. Squeezer

The LIGO squeezed vacuum source, installed for O3 [8], uses spontaneous parametric down-conversion in a subthreshold optical parametric oscillator (OPO) containing a periodically poled potassium titanyl phosphate (PPKTP) nonlinear crystal. The OPO is a traveling-wave, doubly

resonant bow-tie cavity, pumped at 532 nm to produce squeezed vacuum around the interferometer carrier frequency at 1064 nm [38–40]. With the expectation that backaction could be mitigated by frequency-dependent squeezing injection, the OPO cavity finesse and green pump optics were upgraded to generate higher squeezing levels in preparation for O4.

B. Filter cavity

Squeezed vacuum then undergoes a frequency-dependent phase shift upon reflection from a 300-m, in-vacuum, optical filter cavity, producing a frequency-dependent rotation of the squeezed state for frequencies within the cavity resonance. The filter cavity has a full-width-half-maximum linewidth of about 74 Hz and a detuning from carrier of approximately 35 Hz to impart a squeezing rotation that counters the optomechanical response of the interferometer (Fig. 1) while minimizing squeezing loss [26,30].

The system is further engineered [26] to suppress noise from stray interferometer light that is misdirected along the squeezing injection path and, subsequently, scattered back to the interferometer readout by vibrations of the filter cavity and squeezer optics. Both cavity mirrors use triple pendulum suspensions [41] mounted on isolated in-vacuum optical tables [42] for vibration isolation, while relay optics use either single or double suspensions [43]. For filter cavity length stabilization, the scheme developed for LIGO in Ref. [23] is used and further described in Appendix A. Measured filter cavity parameters are presented in Sec. V and discussed in Appendix B.

C. Improved components

In O3, the measured shot noise reduction with squeezing was limited both by the amount of generated squeezing and by propagation losses [8,44]. In particular, the Faraday isolators were a major source of squeezing loss but are necessary to meet LIGO's strict requirements on stray light isolation. In preparation for O4, three custom high-efficiency Faraday isolators were installed, decreasing total loss and improving stray light isolation. In addition to optical losses, mode mismatch between the squeezer and interferometer beams also limited squeezing efficiency in O3 [44]. Active optics [34,35] were installed to improve mode matching between the squeezer, interferometer, and filter cavity. The increased squeezing levels result from these upgrades and are discussed in Sec. V.

D. Long-term stability

The squeezing system is fully automated and integrated with the main interferometer, with the alignment and intensity controls shown in Fig. 3. At the time of writing, both H1 and L1 detectors are operating with frequency-dependent squeezing in O4, demonstrating the stability of the squeezing subsystem on the timescale of weeks.

IV. RESULTS

We present data from the LIGO detectors during the commissioning period preceding O4, between February and May 2023. For these data, the H1 detector operated with approximately 360–380 kW of circulating power in its interferometer arm cavities, while L1 operated with approximately 300 kW; in comparison, the arm power during O3 was 200–230 kW. The strain noise amplitude spectral density of both detectors is shown in Fig. 2.

With frequency-dependent squeezing, we achieved a quantum enhancement of the detectors that simultaneously reduced both shot noise and quantum radiation pressure noise. Compared to the measured detector noise without squeezing (Fig. 2, black) and the detector noise with frequency-independent squeezing (Fig. 2, green), frequency-dependent squeezing provided broadband improvement (Fig. 2, purple), with measurable reductions in the total detector noise from several kilohertz down to frequencies as low as 60 Hz in H1 and 30 Hz in L1.

In the shot-noise-limited region around 1 kHz, both detectors measured higher squeeze levels than O3, due to the higher generated squeezing levels and reduced cumulative optical losses along the squeezing path. In the H1 detector, squeezing reduced the shot noise amplitude by a factor of 1.6 (4.0 dB) near 1 kHz; in the L1 detector, the shot noise reduction was a factor of 1.9 (5.8 dB). Since shot noise is the largest noise source in the kilohertz frequency band, the total interferometer noise was similarly reduced.

While these kilohertz noise improvements are essential to study the postmerger physics of binary neutron stars [45,46], the injection of frequency-independent squeezing significantly degraded detector performance around 100 Hz, which is detrimental to standard metrics of astrophysical sensitivity. For gravitational-wave detectors, a standard figure of merit is the distance to which a binary neutron star (BNS) or binary black hole (BBH) merger can be detected [47,48]; such metrics heavily weigh the detector noise around 100 Hz. As a result, the frequency-independent squeezing spectra corresponded to a 10%–15% reduction in BNS range, compared to no squeezing.

In contrast, frequency-dependent squeezing recovered low-frequency sensitivity, improving the BNS inspiral range by 15%–18% and the BBH inspiral range by 12%, with respect to no squeezing. Since event rates scale with the volume of the observed Universe, this corresponds to an increase of up to 65% in BNS detection rates and 40% in BBH detection rates.

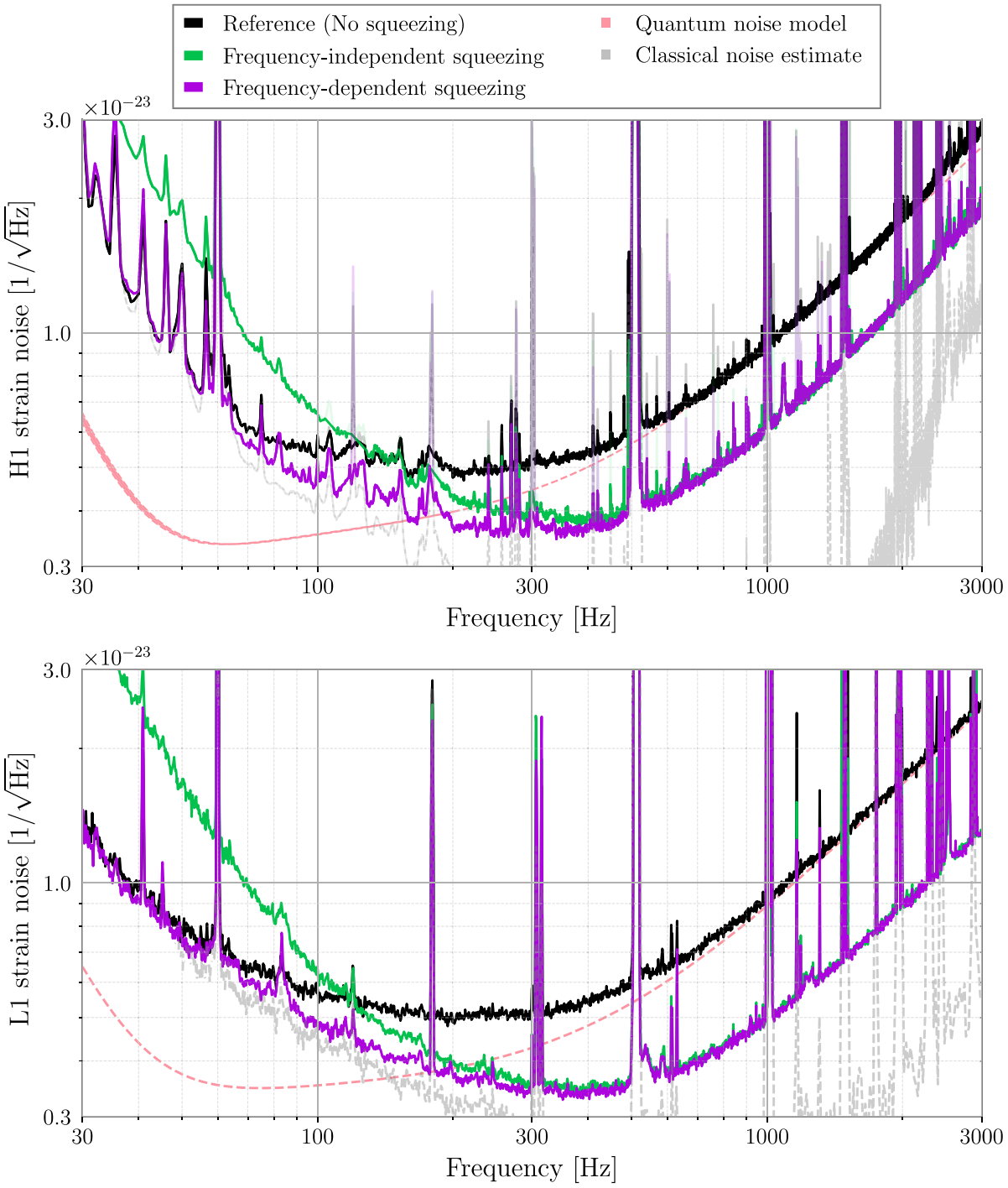

FIG. 2. Observation of frequency-dependent squeezing in the LIGO detectors. The top and bottom show strain noise spectra of the LIGO Hanford (H1) and Livingston (L1) detectors in amplitude spectral density units, measured in the commissioning period leading up the fourth observing run, O4. Reference measurements of detector noise spectra without squeezing are shown in black and measured with the squeezed beam diverted away from the detector. Without squeezing, the classical noise estimate (gray), i.e., the sum of nonquantum noises, is obtained by subtracting the calculated quantum noise (red) from the measured detector noise (black). Frequency-independent squeezing spectra (green) are measured with the squeezed beam injected and the filter cavity end mirror misaligned, to have the input mirror act as a high reflector. With frequency-independent squeezing, shot noise reductions of 4.0 (H1) and 5.8 dB (L1) are observed around 1 kHz, alongside the corresponding increase in quantum radiation pressure noise below a few hundred hertz. Frequency-dependent squeezing spectra (purple) are obtained by locking the filter cavity near resonance, demonstrating the broadband reduction of detector quantum noise. In addition to the squeezed shot noise reduction, the filter cavity reduces total detector noise by 1–2 dB from 60–100 Hz in both detectors, with quantum enhancement visible from kilohertz down to tens of hertz.

TABLE I. Summary of key parameters, including generated squeeze levels, squeezing injection and readout efficiencies, and filter cavity parameters. The observed squeezed shot noise reduction at 1 kHz is used to infer a lower bound on the total squeezing throughput. Entries marked by an asterisk were determined by comparing squeezing data to a quantum noise model. For a full list of parameters, see Table II.

	H1	L1
Squeezing generation		
Generated squeezing	16.9 dB	17 dB*
Measured squeezing	−4.0 dB	−5.8 dB
Squeezing injection efficiency	91.6%	91.8%
Readout efficiency	91%	94%
Phase noise (rms)	<20 mrad	<20 mrad
Total expected throughput	84%	86%
Inferred throughput	>63%	>77%
Filter cavity parameters		
Filter cavity length	297.77 m	297.72 m
Filter cavity detuning	−36 Hz*	−29 Hz*
Filter cavity full linewidth	74 Hz	74 Hz
Filter cavity round-trip loss	<50 ppm	<50 ppm

V. CHARACTERIZATION

The effective quantum noise reduction with squeezing, or the observed squeeze level, is determined by the amount of generated squeezing and by degradation mechanisms such as phase noise, optical loss, and mode mismatch [27,29,30,44]. As a result, the measured squeezing in decibels, N_{dB}, is limited to approximately [44]

$$N_{\mathrm{dB}} \geq 10\log_{10}(2\theta_{\mathrm{rms}} + \Lambda). \tag{7}$$

θ_{rms} is the radians of root-mean-square (rms) phase noise in squeeze angle. Λ is the total fractional optical power loss along the squeezer path, while the efficiency, or optical throughput, is $1-\Lambda$. Table I summarizes the squeezing parameters in the two detectors, including estimates of the throughput and key filter cavity parameters while operating with frequency-dependent squeezing. Appendix C and Table II contain more detail.

A. Phase noise

Phase fluctuations between the squeezer and interferometer fields at the readout, known as "phase noise," reduce the measured squeeze level by mixing some of the orthogonal "antisqueezed" quadrature into the measurement quadrature [8,50,51]. Using the coherent control scheme [52] described in Appendix A, phase noise is controlled to less than 20 mrad in both detectors, as inferred from in-loop error signals and from sweeps of the generated squeezing levels using a diagnostic homodyne detector. Filter cavity detuning fluctuations contribute an additional frequency-dependent phase noise within the cavity bandwidth. At both detectors, this detuning is stabilized to within 1 Hz (i.e., cavity length is stabilized to within 1 pm), adding approximately 5 mrad of excess phase noise around the detuning frequency. Overall, at the current levels of generated squeezing, 20 mrad of rms phase noise reduces measured squeezing by less than 0.2 dB.

B. Optical losses

The primary degradation mechanism that limits the benefit of squeezing is caused by optical losses. Losses mix squeezed vacuum (giving rise to S_h^{SQZ}) with unsqueezed vacuum (S_h^{QN}), limiting the quantum noise reduction in decibels to approximately $N_{\mathrm{dB}} \approx 10\log_{10}[S_h^{\mathrm{SQZ}}(1-\Lambda)/S_h^{\mathrm{QN}} + \Lambda]$. Losses can be separated into two categories: the injection losses that affect the squeezed beam before entering the interferometer and the readout losses in the optical path from the signal extraction mirror to the readout photodetectors. Optical components in the squeezing injection path have been engineered to maximize throughput, achieving >91% injection efficiency measured at both sites. Filter cavities at both sites are measured to have <50 ppm of round-trip loss which, near resonance (around 35 Hz), contributes an additional 10% of squeezing loss [see Eqs. (53) and (57) in Ref. [44]]. At the interferometer output, readout losses limit throughput of both the interferometer signal and the measured squeeze level. These losses are largely common to the interferometer and squeezer and inform our estimate of classical noise. Based on independently measured optical losses at the output port, readout efficiencies of up to 91% (H1) and 94% (L1) are expected.

Given known optical losses, the total expected throughput is similar for both detectors: 84% in H1 and 86% in L1 (see Table I). However, minimum squeezing throughputs of 63% in H1 and 77% in L1 are inferred from measured squeezing levels, i.e., the measured shot noise power reduction with squeezing at 1 kHz of 4.0 dB in H1 and 5.8 dB in L1, while assuming 20 mrad of phase noise.

C. Mode mismatch

Both detectors have a discrepancy between known losses and losses inferred from the measured shot noise reduction. The remaining losses amount to approximately 25% in H1 and approximately 10% in L1. These are likely dominated by residual mode mismatch and misalignment between the squeezed field, the interferometer cavities, and the output mode cleaner cavity. In H1, this hypothesis is supported by estimations of the squeeze level after classical noise subtraction, where the quantum noise reduction from 100–200 Hz is higher, at 4.8 dB, suggesting that unknown losses are frequency dependent and, thus, likely due to mode mismatch of the squeezer and interferometer, as

previously observed [44]. In L1, adjustments of the squeezer alignment and mode matching are routinely performed to optimize measured squeeze levels.

VI. CONCLUSIONS AND OUTLOOK

Frequency-dependent squeezing via a filter cavity enabled a broadband reduction of quantum noise and a significant sensitivity improvement in both LIGO detectors. Below 100 Hz, frequency-dependent squeezing improved the interferometer noise by up to 2 dB. Thanks to several upgrades, in particular, higher levels of generated squeezing, low-loss Faraday isolators, and active mode-matching elements, the amount of measured squeezing around 1 kHz increased to 4.0 dB in H1 and 5.8 dB in L1, from the 2–3 dB observed in O3. At the time of writing, both LIGO detectors operate with frequency-dependent squeezing in O4.

Injecting frequency-dependent squeezing in the LIGO detectors not only enables a significant high-frequency sensitivity improvement, but also circumvents backaction noise that impacts low frequencies. It increases the astrophysical event detection rates by up to 65% and is now a new, fundamental technology for gravitational-wave detectors. Notably, without frequency-dependent squeezing, achieving the equivalent sensitivity in L1 would otherwise require a two- to fourfold increase in both the circulating laser power and mirror mass.

Future upgrades in current facilities and proposed next-generation gravitational-wave observatories like Cosmic Explorer [53] and Einstein Telescope [54] all target 10 dB of frequency-dependent squeezing. Ongoing investigations of the squeezing performance in the LIGO detectors defines the path forward for further technology improvements to reach this ambitious goal.

ACKNOWLEDGMENTS

The authors gratefully acknowledge the support of the United States National Science Foundation (NSF) for the construction and operation of the LIGO Laboratory and Advanced LIGO as well as the Science and Technology Facilities Council (STFC) of the United Kingdom, and the Max-Planck-Society (MPS) for support of the construction of Advanced LIGO. Additional support for Advanced LIGO was provided by the Australian Research Council. The authors acknowledge the LIGO Scientific Collaboration Fellows program for additional support. LIGO was constructed by the California Institute of Technology and Massachusetts Institute of Technology with funding from the National Science Foundation and operates under Cooperative Agreement No. PHY-18671764464. Advanced LIGO was built under Grant No. PHY-18680823459. The A+ Upgrade to Advanced LIGO is supported by U.S. NSF Grant No. PHY-1834382 and United Kingdom STFC Grant No. ST/S00246/1, with additional support from the Australian Research Council. The authors thank Dennis Wilken, Vivishek Sudhir, James Lough, and Kim Burtnyk for carefully reading the manuscript.

APPENDIX A: SQUEEZING SYSTEM CONTROL SCHEME

Figure 3 shows a detailed depiction of the frequency-dependent squeezing implementation in LIGO, including its control scheme. Beyond the overview in Fig. 1, this schematic shows the in-air preparation (yellow) of squeezer control signals before their delivery to the vacuum system (blue) via optical fibers. Arrows indicate how various alignment and length control signals are sensed and actuated across the squeezer system.

1. Squeezer controls

Squeezer controls are largely the same as in O3 [8]. The squeezer pump laser is a 1064 nm laser that is frequency stabilized to the main interferometer laser with 100 kHz bandwidth. The in-vacuum OPO is pumped with green 532 nm light produced from the squeezer pump laser using an in-air second harmonic generation (SHG) cavity. Both OPO and SHG cavities are locked to the squeezer laser using Pound-Drever-Hall (PDH) sensing. Two acousto-optic modulators (AOMs), in series, generate an rf sideband at a detuning of 3.125 MHz, known as the coherent locking field (CLF), for coherent control of the squeezing angle [52]. To sense the relative phase between the squeezed field and the interferometer's local oscillator field, the CLF sideband is injected through the OPO and copropagates alongside squeezed vacuum through to the detector readout.

Squeezed vacuum is generated in the OPO cavity and reflected off the filter cavity that is detuned slightly off resonance. This applies a frequency-dependent phase shift upon reflection to produce frequency-dependent squeezed vacuum. A movable beam diverter opens to inject squeezing at the output port of the interferometer via the output Faraday isolator. When the interferometer is fully locked, the squeezed beam enters and exits the interferometer from the signal extraction cavity, copropagates with the main interferometer beam through the output mode cleaner (OMC), and is detected at the readout photodetectors. For squeeze angle control, the readout photodetector signals are demodulated at the CLF frequency to phase lock the squeezed field to the output interferometer field via feedback to the squeezer pump laser.

For long-term stability, the generated squeezing level and control sideband powers are stabilized based on the dc power of the transmitted 532 nm pump and reflected CLF beams, controlled by GAOM3 and AOM2, respectively. To align the squeezer to the interferometer, a pair of wavefront sensors [i.e., demodulated quadrant photodetectors (QPDs)] detects a 1% pickoff between the output Faraday isolator and the OMC, where the CLF at 3.125 MHz beats

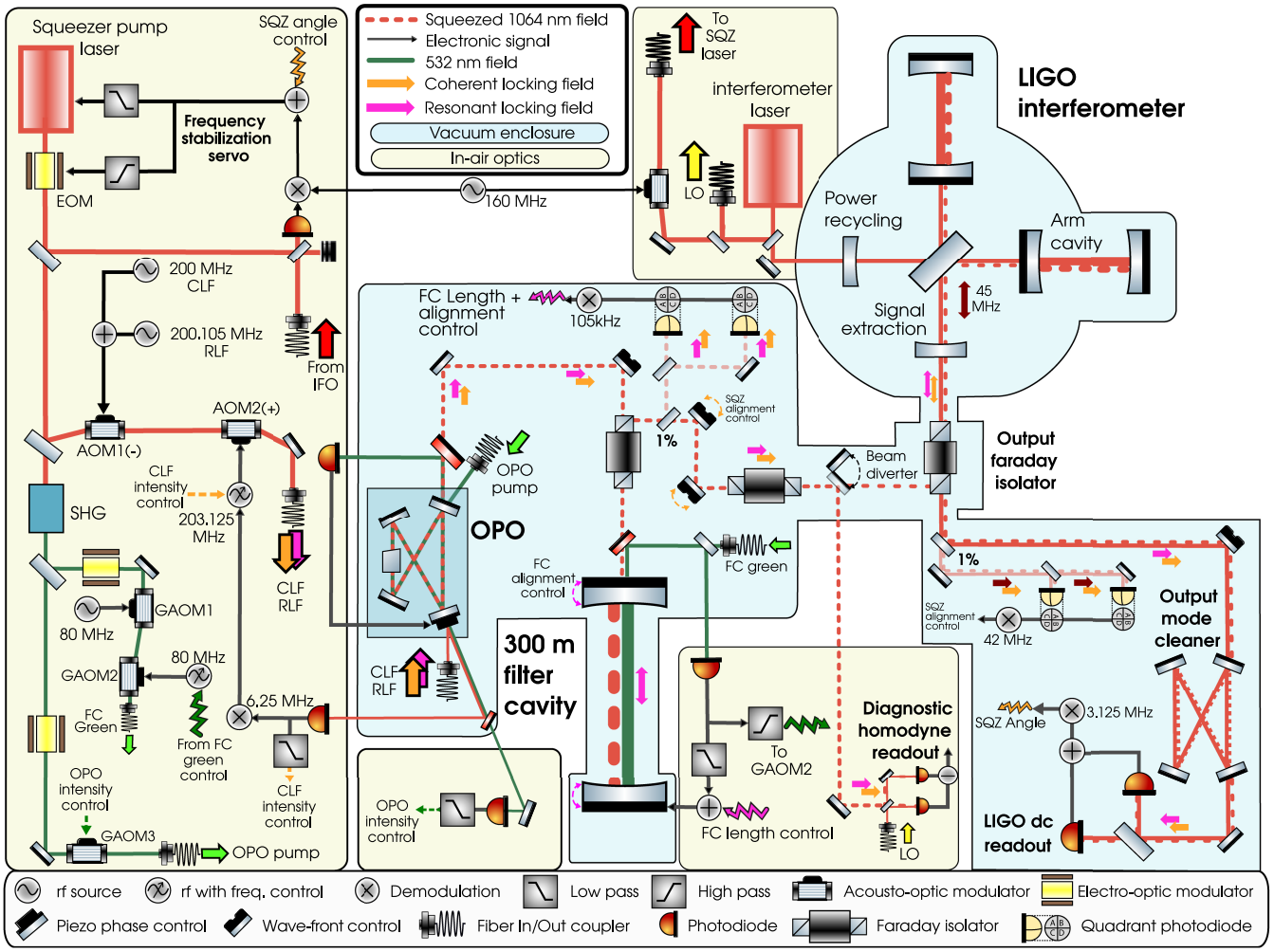

FIG. 3. Detailed optical and controls layout of frequency-dependent squeezing instrumentation in the LIGO detectors, described in Appendix A. To generate squeezed vacuum, the squeezer pump laser is frequency stabilized to the main interferometer laser, frequency doubled using SHG, and sent to pump the in-vacuum OPO. A series of AOMs generate both 1064 nm squeezer control sidebands: the CLF at 3.125 MHz for squeeze angle control [8,52] and the resonant locking field (RLF) at 3.020 MHz for filter cavity length and detuning control [23]. Both sidebands are injected through the OPO and copropagate with squeezed vacuum to the filter cavity, interferometer, and readout photodetectors. A movable beam diverter can redirect the squeezed beam to an in-air balanced homodyne detector for diagnostics. After first acquiring lock at 532 nm, filter cavity length control is transferred to lock on RLF resonance such that the CLF is off resonant; the optical beat note of the RLF and CLF at 105 kHz is, thus, phase sensitive to filter cavity resonance. In reflection of the filter cavity, a 1% pickoff sends this 105 kHz beat note to a pair of quadrant photodiodes for filter cavity length and alignment control. For long-term operation, alignment is controlled between the OPO, filter cavity, and interferometer, and intensity stabilization holds the control sideband powers and generated squeezing levels constant.

with the interferometer sidebands at 45 MHz to produce pitch and yaw alignment signals at 42 MHz. Alignment control signals actuate on the pitch and yaw of a pair of doubly suspended relay optics at the end of the squeezing injection path.

2. Filter cavity control

The filter cavity length control scheme developed for LIGO in Ref. [23] is now in use at both H1 and L1 detectors. Length control of the 298 m high-finesse filter cavity is initially acquired at 532 nm, where the cavity is lower finesse, and subsequently transferred to 1064 nm during nominal operation. The SHG output is split into a secondary path for filter cavity locking; this path contains an electro-optic modulator (EOM) for PDH and a series of two AOMs (GAOM1 and GAOM2) to control the green frequency at the filter cavity. With green PDH sensing, this light is first frequency locked to stabilize the cavity-laser detuning with high bandwidth. This enables the low-bandwidth feedback to the filter cavity mirror suspensions to then bring the physical cavity length under control with length actuation via electromagnet coils along the mirrors' triple suspensions [41].

After locking the cavity length in green, the cavity lock is transferred to resonate a 1064 nm field known as the resonant locking field (RLF), needed for precise control of the detuning between filter cavity resonance and the interferometer carrier frequency ("filter cavity detuning" δ). The RLF is an additional rf sideband generated by the same two AOMs that generate the CLF; unlike the CLF at 3.125 MHz, the RLF is generated at a 3.02 MHz offset from carrier. The RLF frequency is chosen to be near the CLF frequency such that it largely inherits the phase stability of the CLF with respect to interferometer light while still resonating in the filter cavity. This puts the RLF at a 105 kHz offset from the CLF, which is about six free spectral ranges (FSRs) above carrier resonance in the filter cavity $(6 \times \mathrm{FSR} + \delta)$. The RLF and CLF copropagate through the OPO to reach the filter cavity.

The filter cavity length is then locked onto the RLF resonance such that the CLF is off resonant; past the filter cavity, the resonant RLF beats against the off-resonant CLF, producing an error signal at the beat-note frequency of 105 kHz. A 1% optical pickoff for fast, high-gain QPDs is installed in the squeezer path on reflection from the filter cavity; these QPDs have a >120 kHz response and are shot noise limited with only 10 nW per quadrant. These QPDs are demodulated to provide error signals for both length (i.e., detuning) and alignment control of the filter cavity. Length control actuates on the filter cavity end mirror suspension. Alignment control actuates on pitch and yaw of the filter cavity mirrors, aligning the cavity axis to the incident beam from the OPO.

APPENDIX B: FILTER CAVITY CHARACTERIZATION

There are standard methods to characterize a high-finesse optical cavity [55] and, subsequently, its application to frequency-dependent squeezing in gravitational-wave interferometers [27,30,44].

Tables I and II list key optical properties of the high-finesse filter cavities at H1 and L1. The filter cavity length is precisely measured by sweeping an optical sideband to measure the free spectral range [56,57]. The optical storage time in the cavity, which determines the full-width-half-maximum linewidth, is measured using a ringdown technique in both cavity transmission and reflection [55]. From the measured cavity linewidths and the vendor-specified input coupler power transmissivities of 910 ppm, we estimate filter cavity round-trip power losses of 25–50 ppm. Mode mismatch between the squeezed beam from the OPO and the filter cavity is measured by scanning the filter cavity length and measuring the optical modes in transmission using a camera and photodiode power sensor. For this, a bright carrier beam is resonantly transmitted through the OPO in place of the squeezed vacuum beam.

For diagnostic measurements, the squeezed beam is redirected by the in-vacuum squeezer beam diverter to an in-air balanced homodyne detector. The homodyne uses a local oscillator sourced from a fiber pickoff of the main interferometer laser (see Fig. 3, schematic). Figure 4 shows a measurement of frequency-dependent squeezing on the diagnostic homodyne detector, compared to a model [27]. An auxiliary audio field [58] is used to further estimate mode matching and round-trip loss in the filter cavity.

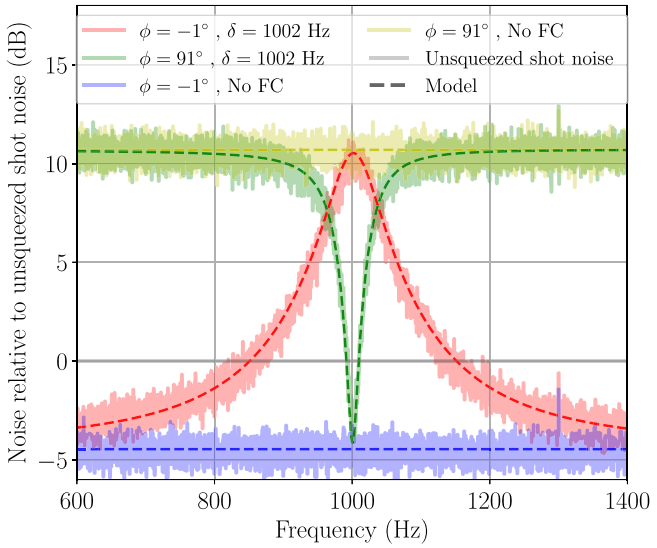

FIG. 4. Frequency-dependent squeezing on a diagnostic balanced homodyne detector in H1. The blue and yellow traces show frequency-independent squeezing spectra measured with the filter cavity end mirror misaligned. The red and green traces show frequency-dependent squeezing spectra, measured with the filter cavity locked at a detuning of $\delta \sim 1$ kHz from the local oscillator. Dotted lines show a model of frequency-dependent squeezing for each configuration, given measured optical properties of the filter cavity [27]. From the model, the plot legend gives the corresponding squeeze angle ϕ and filter cavity detuning δ for each trace.

To reduce quantum radiation pressure noise in the full interferometer, the filter cavity resonance is held at a fixed detuning relative to the carrier light in the interferometer. At both detectors, the filter cavity detuning *in situ* is inferred by comparing detector noise spectra to a quantum noise model. In H1, the detuning is additionally measured using audio-field sweeps on both the homodyne detector and full interferometer [58].

To minimize backscatter driven by the filter cavity, the filter cavity length is stabilized by the RLF locking scheme described in Appendix A to within 1 Hz rms (equivalently, approximately 1 pm rms) at both detectors. In addition, the filter cavity control scheme is designed to minimize frequency noise of the RLF field, as it appears as length noise in the cavity servo. The servo bandwidth to the filter cavity length control servo is cut off at as low a frequency as possible (<50 Hz) such that the sensing noise of the RLF error signal, injected through the servo, does not

compromise the vibration isolation of the triply suspended filter cavity mirrors.

APPENDIX C: INTERFEROMETER AND SQUEEZING PARAMETERS

This appendix discusses the interferometer and squeezing parameters from Sec. V in detail, including a more complete set of parameters in Table II. In particular, we discuss optical losses in two categories: in the squeezing injection path before the interferometer and in the readout path from the interferometer to the photodetectors. We also further describe the interferometer configuration as it relates to the characterization of the measured squeeze levels.

1. Squeezing injection losses

Optical losses in the injection path start from the squeezing generation in the nonlinear crystal. These injection losses include OPO cavity losses, filter cavity losses, and four passes through Faraday isolators before reaching the interferometer, i.e., arriving at the signal extraction mirror. The in-chamber squeezer injection losses are externally measured by injecting a bright carrier field through the OPO in place of the control sidebands; we measure the OPO cavity's optical throughput to be 98.5%–98.7%, in addition to the in-chamber throughput of 93%. Custom low-loss Faraday isolators were implemented in preparation for O4, with measured single-pass throughput on the order of 99%–99.5%. With four isolator passes, through two isolators on the squeezer injection platform (one more than O3) and the interferometer's output Faraday isolator, the O4 isolators provide a significant reduction in losses over those used in O3, which each had 96%–97% single-pass efficiency. In total, known optical losses limit the maximum squeezing injection efficiency to about 91% in both detectors.

To optimize mode matching on the squeezing injection path, three doubly suspended active optics elements, realized by piezodeformable mirrors [34], were installed. The first deformable mirror optimizes mode matching between the OPO and the filter cavity, while the other two mirrors optimize the mode matching of the frequency-dependent squeezed vacuum beam to the interferometer.

TABLE II. Detailed summary of interferometer and squeezer parameters. Entries marked by an asterisk were determined by comparing measured squeezing data to a quantum noise model.

	H1	L1
Interferometer parameters		
Arm power	360–380 kW*	300 kW*
SEC detuning (round-trip phase)	0.54°	0.1°*
Readout angle	−27°	−14°
Readout efficiency		
Optical throughput (SEC to OMC)	97.5%	97.5%
OMC transmission	95.7%	98%
Photodiode quantum efficiency	98%	98%
Total readout efficiency	91%	94%
Squeezing parameters		
Generated squeezing	16.9 dB	17 dB*
Measured squeezing	−4.0 dB	−5.8 dB
Measured antisqueezing	14.4 dB	15.8 dB
OPO throughput	98.5%	98.7%
Injection efficiency (OPO to SEC)	91.6%	91.8%
Phase noise (rms)	<20 mrad	<20 mrad
Total expected throughput	84%	86%
Inferred throughput	>63%	>77%
Filter cavity parameters		
Filter cavity length	297.77 m	297.72 m
Filter cavity detuning	−36 Hz*	−29 Hz*
Filter cavity full linewidth	74 Hz	74 Hz
Filter cavity finesse	6700	6700
Filter cavity round-trip loss	<50 ppm	<50 ppm
Filter cavity mode matching	98%	99.8%
Filter cavity length noise (rms)	<0.5 Hz	<1 Hz

2. Readout losses

Readout losses impact both the shot-noise-limited interferometer sensitivity without squeezing and the total quantum noise reduction achievable with injected squeezing. From the more detailed schematic in Fig. 3, readout losses from the output of the signal extraction mirror to the readout photodetectors include one outgoing pass through the output Faraday isolator, several optical pickoffs required to stabilize alignments between the interferometer and the OMC, optical round-trip losses in the OMC cavity, and the quantum efficiency of the readout photodetectors. Separately, the squeezer and interferometer beams may have different mode matching through the OMC, leading to possible differences in readout loss between the interferometer and squeezer beams. Excluding mode mismatch, the expected readout efficiency is 91% in H1 and 94% in L1.

3. Readout losses without squeezing

Many readout losses are common to the squeezer and interferometer, and, thus, estimating the shot noise level requires knowledge of the interferometer's output losses independent of squeezing. Without squeezing, detector noise around 1 kHz is dominated by shot noise; this level can be compared to a shot noise model [e.g., Eq. (2)] to estimate the *in situ* readout losses, beyond the known optical losses in the path. The shot noise model is primarily determined by the interferometer laser power and optical response, both of which can be independently measured.

Key parameters that characterize the interferometer optical response are the interferometer readout angle and

the detuning of the signal extraction cavity (SEC). Differential losses in the interferometer's arms lead to an imperfect dark fringe with excess field at the output, known as the contrast defect. Since this excess field does not contain information about the differential arm length signal, it results in a nonzero angle between the signal and readout quadratures, which increases the shot noise levels at high frequency [37]. Measuring the residual optical power at the dark fringe of the interferometer provides an upper limit on the readout angle, given in Table II. Next, the SEC detuning, often quoted as the round-trip phase shift through the cavity in degrees, can be estimated by measuring the interferometer response to an external drive of the end mirrors [59]. Given this optical response, the shot noise model without squeezing [37,44] (Fig. 2, red) can be compared to the measured noise spectra without squeezing (Fig. 2, black) to estimate the interferometer readout losses.

Without squeezing, for the L1 detector, we find that less than 10% additional readout losses are needed to explain the observed shot noise level, given the expected optical losses at the output of the interferometer. For H1, a similar analysis of readout losses is complicated by uncertainty in the arm power, a larger SEC detuning, and a larger readout angle as constrained by the contrast defect. For the reported H1 parameters in Table II, we estimate less than 20% additional interferometer readout losses compared to known losses.

For both detectors, the additional interferometer readout losses can be related to mode mismatch. For instance, mode matching of the interferometer output beam through the OMC is imperfect and highly dependent on the thermal state of the interferometer [44]. Another source of mode mismatch is intracavity mismatch between the signal extraction cavity and the two arm cavities, which varies with the thermal state of the interferometer and optical defects across the LIGO's core optics [60]. Work to understand mode mismatch is ongoing.

[1] J. Aasi *et al.*, *Advanced LIGO*, Classical Quantum Gravity **32**, 074001 (2015).

[2] F. Acernese, M. Agathos, K. Agatsuma *et al.*, *Advanced Virgo: A second-generation interferometric gravitational wave detector*, Classical Quantum Gravity **32**, 024001 (2014).

[3] C. M. Caves, *Quantum-mechanical noise in an interferometer*, Phys. Rev. D **23**, 1693 (1981).

[4] L. Barsotti, J. Harms, and R. Schnabel, *Squeezed vacuum states of light for gravitational wave detectors*, Rep. Prog. Phys. **82**, 016905 (2018).

[5] J. Abadie, B. P. Abbott, R. Abbott *et al.*, *A Gravitational Wave Observatory operating beyond the quantum shot-noise limit*, Nat. Phys. **7**, 962 (2011).

[6] H. Grote, K. Danzmann, K. L. Dooley, R. Schnabel, J. Slutsky, and H. Vahlbruch, *First long-term application of squeezed states of light in a Gravitational-Wave Observatory*, Phys. Rev. Lett. **110**, 181101 (2013).

[7] J. Aasi *et al.*, *Enhanced sensitivity of the LIGO gravitational wave detector by using squeezed states of light*, Nat. Photonics **7**, 613 (2013).

[8] M. Tse, H. Yu, N. Kijbunchoo *et al.*, *Quantum-enhanced Advanced LIGO detectors in the era of gravitational-wave astronomy*, Phys. Rev. Lett. **123**, 231107 (2019).

[9] F. Acernese, M. Agathos *et al.* (Virgo Collaboration), *Increasing the astrophysical reach of the Advanced Virgo detector via the application of squeezed vacuum states of light*, Phys. Rev. Lett. **123**, 231108 (2019).

[10] J. Lough, E. Schreiber, F. Bergamin *et al.*, *First demonstration of 6 dB quantum noise reduction in a kilometer-scale Gravitational Wave Observatory*, Phys. Rev. Lett. **126**, 041102 (2021).

[11] H. Yu, L. McCuller, M. Tse *et al.*, *Quantum correlations between light and the kilogram-mass mirrors of LIGO*, Nature (London) **583**, 43 (2020).

[12] F. Acernese, M. Agathos, L. Aiello *et al.* (Virgo Collaboration), *Quantum backaction on kg-scale mirrors: Observation of radiation pressure noise in the Advanced Virgo Detector*, Phys. Rev. Lett. **125**, 131101 (2020).

[13] V. B. Braginskiĭ and Y. I. Vorontsov, *Quantum-mechanical limitations in macroscopic experiments and modern experimental technique*, Sov. Phys. Usp. **17**, 644 (1975).

[14] C. M. Caves, K. S. Thorne, R. W. P. Drever, V. D. Sandberg, and M. Zimmermann, *On the measurement of a weak classical force coupled to a quantum-mechanical oscillator. I. Issues of principle*, Rev. Mod. Phys. **52**, 341 (1980).

[15] V. B. Braginsky, Y. I. Vorontsov, and K. S. Thorne, *Quantum nondemolition measurements*, Science **209**, 547 (1980).

[16] H. P. Yuen, *Contractive states and the standard quantum limit for monitoring free-mass positions*, Phys. Rev. Lett. **51**, 719 (1983).

[17] M. Ozawa, *Measurement breaking the standard quantum limit for free-mass position*, Phys. Rev. Lett. **60**, 385 (1988).

[18] W. G. Unruh, *Readout state preparation and quantum nondemolition*, in *Quantum Optics, Experimental Gravity, and Measurement Theory*, NATO Advanced Science Institutes Series, edited by P. Meystre and M. O. Scully (Springer, Boston, 1983), pp. 637–645.

[19] C. M. Caves, *Quantum-mechanical radiation-pressure fluctuations in an interferometer*, Phys. Rev. Lett. **45**, 75 (1980).

[20] H. J. Kimble, Y. Levin, A. B. Matsko, K. S. Thorne, and S. P. Vyatchanin, *Conversion of conventional gravitational-wave interferometers into quantum nondemolition interferometers by modifying their input and/or output optics*, Phys. Rev. D **65**, 022002 (2001).

[21] S. Chelkowski, H. Vahlbruch, B. Hage, A. Franzen, N. Lastzka, K. Danzmann, and R. Schnabel, *Experimental characterization of frequency-dependent squeezed light*, Phys. Rev. A **71**, 013806 (2005).

[22] E. Oelker, T. Isogai, J. Miller, M. Tse, L. Barsotti, N. Mavalvala, and M. Evans, *Audio-band frequency-dependent squeezing for gravitational-wave detectors*, Phys. Rev. Lett. **116**, 041102 (2016).

[23] L. McCuller, C. Whittle, D. Ganapathy *et al.*, *Frequency-dependent squeezing for Advanced LIGO*, Phys. Rev. Lett. **124**, 171102 (2020).
[24] Y. Zhao, N. Aritomi, E. Capocasa *et al.*, *Frequency-dependent squeezed vacuum source for broadband quantum noise reduction in advanced gravitational-wave detectors*, Phys. Rev. Lett. **124**, 171101 (2020).
[25] F. Acernese *et al.* (Virgo Collaboration), *Frequency-dependent squeezed vacuum source for the Advanced Virgo gravitational-wave detector*, Phys. Rev. Lett. **131**, 041403 (2023).
[26] L. McCuller and L. Barsotti, *Design requirement document of the* a+ *filter cavity and relay optics for frequency dependent squeezing*, LIGO public document, 2019, https://dcc.ligo.org/LIGO-T1800447/public.
[27] P. Kwee, J. Miller, T. Isogai, L. Barsotti, and M. Evans, *Decoherence and degradation of squeezed states in quantum filter cavities*, Phys. Rev. D **90**, 062006 (2014).
[28] M. Evans, L. Barsotti, P. Kwee, J. Harms, and H. Miao, *Realistic filter cavities for advanced gravitational wave detectors*, Phys. Rev. D **88**, 022002 (2013).
[29] F. Ya. Khalili, *Optimal configurations of filter cavity in future gravitational-wave detectors*, Phys. Rev. D **81**, 122002 (2010).
[30] C. Whittle, K. Komori, D. Ganapathy, L. McCuller, L. Barsotti, N. Mavalvala, and M. Evans, *Optimal detuning for quantum filter cavities*, Phys. Rev. D **102**, 102002 (2020).
[31] M. J. Yap, J. Cripe, G. L. Mansell, T. G. McRae, R. L. Ward, B. J. J. Slagmolen, P. Heu, D. Follman, G. D. Cole, T. Corbitt, and D. E. McClelland, *Broadband reduction of quantum radiation pressure noise via squeezed light injection*, Nat. Photonics **14**, 19 (2020).
[32] J. Südbeck, S. Steinlechner, M. Korobko, and R. Schnabel, *Demonstration of interferometer enhancement through Einstein–Podolsky–Rosen entanglement*, Nat. Photonics **14**, 240 (2020).
[33] M. J. Yap, P. Altin, T. G. McRae, B. J. J. Slagmolen, R. L. Ward, and D. E. McClelland, *Generation and control of frequency-dependent squeezing via Einstein–Podolsky–Rosen entanglement*, Nat. Photonics **14**, 223 (2020).
[34] V. Srivastava, G. Mansell, C. Makarem *et al.*, *Piezo-deformable mirrors for active mode matching in Advanced LIGO*, Opt. Express **30**, 10491 (2022).
[35] H. T. Cao, A. Brooks, S. W. S. Ng, D. Ottaway, A. Perreca, J. W. Richardson, A. Chaderjian, and P. J. Veitch, *High dynamic range thermally actuated bimorph mirror for gravitational wave detectors*, Appl. Opt. **59**, 2784 (2020).
[36] H. T. Cao, S. W. S. Ng, M. Noh, A. Brooks, F. Matichard, and P. J. Veitch, *Enhancing the dynamic range of deformable mirrors with compression bias*, Opt. Express **28**, 38480 (2020).
[37] A. Buonanno and Y. Chen, *Quantum noise in second generation, signal-recycled laser interferometric gravitational-wave detectors*, Phys. Rev. D **64**, 042006 (2001).
[38] S. S. Y. Chua, M. S. Stefszky, C. M. Mow-Lowry, B. C. Buchler, S. Dwyer, D. A. Shaddock, P. K. Lam, and D. E. McClelland, *Backscatter tolerant squeezed light source for advanced gravitational-wave detectors*, Opt. Lett. **36**, 4680 (2011).
[39] E. Oelker, G. Mansell, M. Tse, J. Miller, F. Matichard, L. Barsotti, P. Fritschel, D. E. McClelland, M. Evans, and N. Mavalvala, *Ultra-low phase noise squeezed vacuum source for gravitational wave detectors*, Optica **3**, 682 (2016).
[40] A. R. Wade, G. L. Mansell, S. S. Y. Chua, R. L. Ward, B. J. J. Slagmolen, D. A. Shaddock, and D. E. McClelland, *A squeezed light source operated under high vacuum*, Sci. Rep. **5**, 18052 (2015).
[41] M. V. Plissi, C. I. Torrie, M. E. Husman, N. A. Robertson, K. A. Strain, H. Ward, H. Lueck, and J. Hough, *GEO 600 triple pendulum suspension system: Seismic isolation and control*, Rev. Sci. Instrum. **71**, 2539 (2000).
[42] F. Matichard, B. Lantz, R. Mittleman *et al.*, *Seismic isolation of Advanced LIGO: Review of strategy, instrumentation and performance*, Classical Quantum Gravity **32**, 185003 (2015).
[43] Á. Fernández-Galiana, L. McCuller, J. Kissel *et al.*, *Advanced LIGO squeezer platform for backscattered light and optical loss reduction*, Classical Quantum Gravity **37**, 215015 (2020).
[44] L. McCuller, S. E. Dwyer, A. C. Green *et al.*, *LIGO's quantum response to squeezed states*, Phys. Rev. D **104**, 062006 (2021).
[45] J. A. Clark, A. Bauswein, N. Stergioulas, and D. Shoemaker, *Observing gravitational waves from the post-merger phase of binary neutron star coalescence*, Classical Quantum Gravity **33**, 085003 (2016).
[46] K. Chatziioannou, J. A. Clark, A. Bauswein, M. Millhouse, T. B. Littenberg, and N. Cornish, *Inferring the post-merger gravitational wave emission from binary neutron star coalescences*, Phys. Rev. D **96**, 124035 (2017).
[47] H.-Y. Chen, D. E. Holz, J. Miller, M. Evans, S. Vitale, and J. Creighton, *Distance measures in gravitational-wave astrophysics and cosmology*, Classical Quantum Gravity **38**, 055010 (2021).
[48] Calculation of the BNS range uses a standard $1.4M_\odot$ template for the coalescence of two $1.4M_\odot$ neutron stars. Calculation of the BBH range uses a $30M_\odot$ template, which is representative of a typical BBH merger [49].
[49] B. P. Abbott *et al.* (LIGO Scientific Collaboration and Virgo Collaboration), *GWTC-1: A gravitational-wave transient catalog of compact binary mergers observed by LIGO and Virgo during the first and second observing runs*, Phys. Rev. X **9**, 031040 (2019).
[50] S. Dwyer, L. Barsotti, S. S. Y. Chua *et al.*, *Squeezed quadrature fluctuations in a gravitational wave detector using squeezed light*, Opt. Express **21**, 19047 (2013).
[51] N. Kijbunchoo, T. McRae, D. Sigg *et al.*, *Low phase noise squeezed vacuum for future generation gravitational wave detectors*, Classical Quantum Gravity **37**, 185014 (2020).
[52] H. Vahlbruch, S. Chelkowski, B. Hage, A. Franzen, K. Danzmann, and R. Schnabel, *Coherent control of vacuum squeezing in the gravitational-wave detection band*, Phys. Rev. Lett. **97**, 011101 (2006).
[53] M. Evans, R. X. Adhikari, C. Afle *et al.*, *A horizon study for cosmic explorer: science, observatories, and community*, arXiv:2109.09882.

[54] M. Punturo *et al.*, *The Einstein Telescope: A third-generation Gravitational Wave Observatory*, Classical Quantum Gravity **27**, 194002 (2010).

[55] T. Isogai, J. Miller, P. Kwee, L. Barsotti, and M. Evans, *Loss in long-storage-time optical cavities*, Opt. Express **21**, 30114 (2013).

[56] A. Staley, D. Hoak, A. Effler, K. Izumi, S. Dwyer, K. Kawabe, E. J. King, M. Rakhmanov, R. L. Savage, and D. Sigg, *High precision optical cavity length and width measurements using double modulation*, Opt. Express **23**, 19417 (2015).

[57] M. Rakhmanov, M. Evans, and H. Yamamoto, *An optical Vernier technique for in situ measurement of the length of Long Fabry-Pérot cavities*, Meas. Sci. Technol. **10**, 190 (1999).

[58] D. Ganapathy, V. Xu, W. Jia, C. Whittle, M. Tse, L. Barsotti, M. Evans, and L. McCuller, *Probing squeezing for gravitational-wave detectors with an audio-band field*, Phys. Rev. D **105**, 122005 (2022).

[59] L. Sun, E. Goetz, J. S. Kissel *et al.*, *Characterization of systematic error in Advanced LIGO calibration*, Classical Quantum Gravity **37**, 225008 (2020).

[60] A. F. Brooks, B. Abbott, M. A. Arain *et al.*, *Overview of Advanced LIGO adaptive optics*, Appl. Opt. **55**, 8256 (2016).